Journal of Fluid Science and Technology

Vol. 7, No. 3, 2012

Numerical Investigations of Slip Effects on Rarefied Gas Flows by First and Second-Order Slip Boundaries*

Youichi OGATA** and Koudai MATSUMOTO**

**Department of Mechanical System Engineering, Hiroshima University,
1-4-1, Kagamiyama, Higashi Hiroshima-shi, Hiroshima 739-8527, Japan
E-mail: yogata@hiroshima-u.ac.jp

Abstract

This paper discusses comparisons of first and second-order slip boundary conditions on the range of Knudsen numbers of some typical MEMS as $O(10^{-3}) < Kn < O(10^{-1})$ by numerical simulations using the continuum model based on the Navier-Stokes (N-S) equations. Slip flows are solved by the Constrained Interpolation Profile (CIP) method. A numerical method for a simple but general form of a slip boundary condition on a simple planar wall is also introduced. Numerical solutions are in very good agreement with exact solutions of the N-S equations with slip boundaries in two-dimensional Poiseuille flows in the hard sphere (HS) model. The present numerical method is next applied to two and three-dimensional rid-driven cavity flows, employing slip coefficients for the Bhatnagar-Gross-Krook (BGK) model. The results indicate differences of slip effects near walls between the first and second-order slip boundary can also affect whole streamlines and velocity distributions in a closed region with increasing the Knudsen number.

Key words: CIP Method, Navier-Stokes, Slip Flows, Rarefied Gas, Micro-Fluids

1. Introduction

The importance of investigations of micro-gas-flows has been increasing owing to developments of microdevices such as micro-electro-mechanical systems (MEMS). The Knudsen number defined as $Kn \equiv \lambda / L$ has to be taken into account to investigate properties of such flows, where λ is the mean free path of a gas and L is a characteristic length. This is because the number is one of the most important characteristic measures to determine degrees of rarefaction of gases. Therefore, appropriate approaches have to be carefully selected depending on the range of the Knudsen number.

The Boltzmann equation for the velocity distribution function in phase space is required to investigate flows over the wide range of the Knudsen number, and the direct simulation Monte Carlo (DSMC) method has been effective to compute the collision term accurately[1,2]. On the contrary, some kinds of numerical approaches using discrete grid points in phase space such as finite difference schemes[3,4] have been also proposed to the Boltzmann equation. In order to reduce calculations of integrals in the collision term of the Boltzmann equation, some kinetic-type models such as the Bhatnagar-Gross-Krook (BGK) equation[5] have been also used widely.

However, the Knudsen number in some typical MEMS such as micro pumps is about $O(10^{-3}) < Kn < O(10^{-1})$[6], which is called the slip flow regime. We can employ continuum models based on the Navier-Stokes (N-S) equations in conjunction with slip velocity boundary conditions at walls for slip flows[7,8] instead of kinetic-type models. Maxwell first

*Received 7 Feb., 2012 (No. 12-0102)
[DOI: 10.1299/jfst.7.374]

brought forward the first-order slip boundary for tangential velocity on a simple planar wall[9], and higher-order boundary conditions have been also proposed as its improvement. One of the authors has numerically obtained some fundamental results for the Maxwell's first-order slip boundary using the Constrained Interpolation Profile (CIP) method[10,11,12]. It is the robust and less diffusive solver for hyperbolic equations with accuracy of third-order both in time and space; a lot of successful results such as fluid-structure interactions have been introduced[11]. It has been also indicated in the previous paper that the N-S equations of incompressible flows with the slip boundary are comparable with kinetic-approaches for the slip regime through some conventional benchmark tests[12] .

This paper is intended to show an extension of the numerical method in Ref. 12 from the Maxwell's slip boundary condition to a general form which represents first and second-order slip boundary conditions, and to compare slip effects of both slip conditions on flows in an opened and a closed area. Basic equations are briefly reviewed and a numerical method for a general form of slip boundary conditions is implemented in Section 2. The present method is validated through the Poiseulle flow as a benchmark test in Section 3.1. Next, two and three-dimensional lid-driven cavity flows are solved to compare slip and rarefaction effects on multi-dimensional flows between first and second-order slip boundaries in Sections 3.2 and 3.3, respectively. Concluding remarks are in Section 4.

2. Numerical procedures for slip flow regime

2.1 Basic equations

In this paper, the Knudsen number is assumed to be finite but small as a slip flow. In particular, the flow is assumed to be incompressible and isothermal because we will deal with the flow of which a reference speed is much lower than a thermal velocity; the Mach number is much smaller than unity and the change of gas density is negligible to hardly have an effect on flow fields. The reference temperature of the gas is formally defined as T_0 . Dimensionless quantities are defined as follows:

$$\hat{\mathbf{x}} = \mathbf{x}/h_0 , \quad \hat{t} = t/t_0 , \quad \hat{\rho} = \rho/\rho_0 , \quad \hat{\mathbf{u}} = \mathbf{u}/U_0 , \quad \hat{p} = p/p_0 , \tag{1}$$

where $\rho, \mathbf{u} = (u, v, w)$ and p are the density, macroscopic velocity and pressure, respectively. The reference length, velocity, time, density and pressure are $h_0 , U_0 , t_0 = h_0/U_0 , \rho_0$ and $p_0 = \rho_0 U_0^2$, respectively. The reference viscosity coefficient μ_0 and the reference thermal velocity C_0 are described as follows:

$$\mu_0 = \alpha \lambda_0 p_0 \sqrt{\frac{2}{\pi R T_0}} , \quad C_0 \equiv \sqrt{2RT_0} , \tag{2}$$

where R is the gas constant and λ_0 is the mean free path. The dependence of μ_0 on collision models can be included in the coefficient α . For example, the hard-sphere (HS) and BGK models have $\alpha = 5\pi/16 (\cong 1.0)$[13] and $\alpha = \pi/4$[14,15], respectively.

The quantities (μ_0, λ_0, C_0) are also assumed to be constant in the whole flow field because of the assumption of the incompressible and isothermal flow. A relationship between the Knudsen number Kn and the Reynolds number Re can be readily found through the Mach number Ma and Eq. (2) as follows[14,15]:

$$\frac{1}{Ma} \equiv \frac{C_0}{U_0} , \quad Kn \equiv \frac{\lambda_0}{h_0} , \quad \frac{1}{Re} \equiv \frac{\mu_0}{\rho_0 h_0 U_0} = \frac{\alpha}{\sqrt{\pi}} \frac{Kn}{Ma} . \tag{3}$$

The Reynolds number is small for a large Knudsen number with a fixed Mach number. However, flows for large Knudsen numbers will be different from nonslip continuum flows for low Reynolds numbers if there are walls, owing to the slip on walls. The ``^" sign used in Eq. (1) to represent dimensionless variables is dropped here for simple notation, then, the dimensionless N-S equations can be described on the basis of Eqs. (1) to (3) as follows:

$$\nabla \cdot \mathbf{u} = 0\,, \tag{4}$$

$$\frac{\partial \mathbf{u}}{\partial t} + (\mathbf{u} \cdot \nabla)\mathbf{u} = -\nabla p + \frac{1}{Re}\nabla^2 \mathbf{u}\,. \tag{5}$$

Equations (4) and (5) are solved by the CIP-Combined Unified Procedure (CUP) method with a fractional step[12,16]. The left-hand side of Eq. (5) called the advection phase is solved by the rational function CIP method[17] in multidimensions[18,19] for monotone preserving in this paper. The right-hand side called the nonadvection phase is solved after the advection phase. The viscosity term is solved using the implicit scheme with the second-order finite difference, and the Poisson equation of the pressure for the condition Eq. (4) is solved using the Bi-CGSTAB method. Next, we discuss how to appropriately make a formulation of a higher-order slip boundary condition, which uses the N-S solution of velocity $\mathbf{u}$ on a planar wall.

2.2 Slip boundary condition for tangential velocity on a planar wall

When we consider an interaction between a slip gas flow and a planar wall with a tangential velocity u_W in the N-S equations, it is effective that velocity slip conditions are imposed at a point $\mathbf{x}_W$ on the wall surface. In contrast to Maxwell's first-order slip boundary condition[9], a second-order slip model was first brought forward by Cercignani[20]. The second-order velocity slip condition is as follows:

$$\Delta U_{slip} = u_{\mathbf{x}=\mathbf{x}_W} - u_W = A_1 Kn\left(\frac{\partial u}{\partial n}\right)_{\mathbf{x}=\mathbf{x}_W} - A_2 Kn^2\left(\frac{\partial^2 u}{\partial n^2}\right)_{\mathbf{x}=\mathbf{x}_W}\,, \tag{6}$$

where n is the coordinate, and $\partial/\partial n$ and $\partial^2/\partial n^2$ are the first and second-order spatial derivative normal to the planar wall, respectively. ΔU_{slip} is a tangential slip velocity of the gas on the wall. The coefficient A_1 is 1.0 in the original Maxwell's condition when the accommodation coefficient $\sigma = 1.0$. However, accurate solutions of the linearized Boltzmann equation (LBE) give $A_1 = 1.11$ in $\sigma = 1.0$ for the HS model[21]; the coefficient A_1 includes the Knudsen layer correction.

Several pairs of coefficients (A_1, A_2) have been proposed depending on collision and mathematical models. For example, the Taylor Expansion-based model can give $(A_1, A_2) = (1.0, 0.5)$[22]. In order to find the tangential gas velocity $u_{\mathbf{x}=\mathbf{x}_W}$ consistent with Eq. (6) on the wall, a profile of a tangential velocity component f near a planar wall is assumed to be represented by a quadratic interpolation function as follows:

$$f(n) = an^2 + bn + c\,. \tag{7}$$

For example, let us consider the wall at $y = 0.0$ with a wall speed u_W in x-direction in two-dimensions (see Fig. 1, then $f = u$ and $n = y$ in Eq. (7)). The coefficients (a, b, c) satisfying Eq. (6) at $(x, y) = (x_i, 0)$ can be obtained by the following conditions using the three grid points on and near the wall:

$$u_{i,2} = a(\Delta y_1 + \Delta y_2)^2 + b(\Delta y_1 + \Delta y_2) + c, \tag{8}$$

$$u_{i,1} = a\Delta y_1^{\,2} + b\Delta y_1 + c, \tag{9}$$

$$u_{i,0} = c = u_w + A_1 Kn \cdot b - A_2 Kn^2 \cdot 2a, \tag{10}$$

where $\Delta y_j (j = 1,2)$ is the mesh size. Thus, the coefficients (a, b) can be easily obtained by putting Eq. (10) into Eqs. (8) and (9) as follows:

$$\begin{pmatrix} a \\ b \end{pmatrix} = \frac{1}{\alpha_{11}\alpha_{22} - \alpha_{12}\alpha_{21}} \begin{pmatrix} \alpha_{22} & -\alpha_{12} \\ -\alpha_{21} & \alpha_{11} \end{pmatrix} \begin{pmatrix} u_{i,2} - u_w \\ u_{i,1} - u_w \end{pmatrix}, \tag{11}$$

$$\alpha_{11} = (\Delta y_1 + \Delta y_2)^2 - 2A_2 Kn^2, \quad \alpha_{12} = \Delta y_1 + \Delta y_2 + A_1 Kn,$$

$$\alpha_{21} = \Delta y_1^{\,2} - 2A_2 Kn^2, \quad \alpha_{22} = \Delta y_1 + A_1 Kn. \tag{12}$$

Hence, the tangential gas velocity on the wall $u_{i,0} = c\left(= u_{\mathbf{x}=\mathbf{x}_w}\right)$ can be determined by Eqs. (10) to (12). Even if a wall is placed at $j = jmax$ which is the maximum number of grid points in y-direction, Eqs. (8) to (12) can also give the tangential gas velocity $u_{i,jmax}$ by just replacing $(\Delta y_1, \Delta y_2)$ and $(u_{i,1}, u_{i,2})$ with $(\Delta y_{jmax}, \Delta y_{jmax-1})$ and $(u_{i,jmax-1}, u_{i,jmax-2})$, respectively. Note that, in $A_2 = 0$, the coefficients (a, b, c) result in the ones for the first-order slip boundary. Even in three-dimensions, z-component of the gas velocity $w_{\mathbf{x}=\mathbf{x}_w}$ can be straightforwardly obtained by replacing u with w in Eqs. (8) to (11).

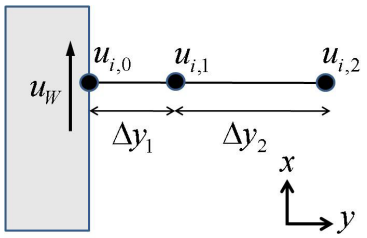

Fig. 1 Grid points for a tangential velocity component on and near a wall in xy-plane.

Though slip boundary conditions are derived under assumptions of steady flows, they can be also applied to quasi-static flows, i.e, collision time $\tau_c \cong \lambda_0 / C_0$ is much smaller than characteristic time $T \cong h_0 / U_0$, or $Kn \cdot Ma$ is much smaller than the unity. Slip models for time-dependent flows have been validated by Hadjiconstantinou[23]. Meanwhile, we need to care about two following points using slip boundaries.

First, true profiles for slip/transitional flows can be expressed as the combination of N-S solution part (u_{NS}) with Knudsen layer part (u_{Kn}), $u_{true} = u_{NS} + u_{Kn}$; u_{Kn} becomes zero out of the layer[24]. Three grid points used for Eq. (7) may be inside the layer in $Kn \cong O(10^{-1})$. However, Eq. (7) cannot include the structure of the Knudsen layer part u_{Kn} because Eq. (5) can give only u_{NS} even in the layer. Therefore, while fictitious slip boundary conditions have been suggested[8,14,25] so that flow field outside the Knudsen layer can be correctly captured by corrections of slip boundary coefficients even though u_{Kn} rapidly decreases inside the Knudsen layer, the range of Knudsen numbers for slip boundary conditions should be practically restricted in $Kn \lesssim O(10^{-1})$ as has been suggested[2].

Second, Sone has established the general formulations of the slip boundary by the asymptotic theory[14,15,26,27]. When the tangential gas velocity changes along a wall, Eq. (6) will be incorrect because, exactly, tangential shear stress has to be considered. One of improved solutions is the Maxwell-Burnett slip law[28]. In addition, slip of the normal velocity component will also take place by the second-order term in a power series of Kn for Grad-Hilbert solution and Knudsen layer part[14,15].

Therefore, we set the following assumptions to use Eq. (6) for all calculations in the present paper. First, slip of the normal velocity on a planar wall is not taken into account, that is, the nonslip boundary condition is imposed for the normal velocity. The assumption is correct in the first-order approximation of the normal slip velocity[14,15], and the slip boundary for the tangential velocity in the second-order term reduces to Eq. (6) if the second-order term of the normal velocity slip is small for small Knudsen numbers.

Next, effects of sharp corners in a closed area such as a cavity containing a flow are not considered as Ref. 12. When a wall has a curvature κ, Eq. (6) is also insufficient because terms including κ have to be also added to slip boundary conditions. However, Aoki *et al.* have discussed discontinuity of the velocity distribution function caused by the sharp corner[29], and shown that the discontinuity is very small for small Kn when the velocity distribution function becomes almost a local Maxwellian near the corner. In addition, a grid point at a corner is not used to solve the N-S equations and to make the interpolation function Eq. (7) in numerical simulations. All calculations in the present paper are devoted to flows on simple planar walls and no term of κ is treated in Eq. (6).

Next section, the present method Eqs. (7) to (12) for Eq. (6) as the velocity boundary condition will be briefly verified using the Poiseuille flow in the HS model.

3. Numerical experiments of the slip flow regime

3.1 Poiseuille flow

The plane Poiseuille flow between two parallel plates has been investigated in views of theory and experiments very well. For example, Ohwada *et al.* have obtained comprehensive solutions of mass flows and velocity profiles for the HS model using the LBE; the solutions agree with experiments very well[21]. In the continuum model, Hadjiconstantinou has suggested coefficients $(A_1, A_2) = (1.11, 0.61)$ in Eq. (6) for the HS model[24] based on solutions of Ref. 21. Hence, the flow is a proper benchmark test to make sure the validity of the present method.

A channel width H is taken as the reference length $(h_0 = H)$, thus the Knudsen number is defined as $Kn \equiv \lambda / H$. A parameter $k \equiv (\sqrt{\pi}/2) Kn$ is introduced to directly compare numerical solutions to Ref. 21. A gas confined between two parallel stationary plates is driven by pressure gradient along the two plates. The inlet and outlet pressures are fixed to $p_{in} = 1.0$ and $p_{out} = 1.0 - 1.0 \times 10^{-5}$ in this test, respectively.

The number of grid points are $(N_x, N_y) = (50, 50)$ and the computational regions are $(0 \le x \le 2), (-1/2 \le y \le 1/2)$. The x and y spaces are divided into uniform section with $\Delta x = 0.04$ and nonuniform sections with the minimum width $\Delta y_{\min} = 6.175 \times 10^{-3}$ near the walls and the maximum width $\Delta y_{\max} = 4.568 \times 10^{-2}$ around $y = 0$, respectively.

Exact solutions of the mass flow rate Q_M and velocity profile $u(y)$ for the HS model in Eq. (3), the accommodation coefficient $\sigma = 1.0$ and the slip velocity boundary Eq. (6), can be described as follows:

$$\frac{u}{u^*} = \frac{4}{5\sqrt{\pi} Kn} \left[Kn(A_1 + 2A_2 Kn) - (y + 1/2)^2 + y + 1/2 \right], \tag{13}$$

$$\frac{Q_M}{\rho u^* H} = \frac{2}{15\sqrt{\pi} Kn} \left(1 + 6A_1 Kn + 12 A_2 Kn^2 \right), \tag{14}$$

where $u^* = -C_0 \, dp/dx$ and $dp/dx = (p_{out} - p_{in})/H/2$; both solutions reduce to those of the first-order boundary for $A_2 = 0$ [13].

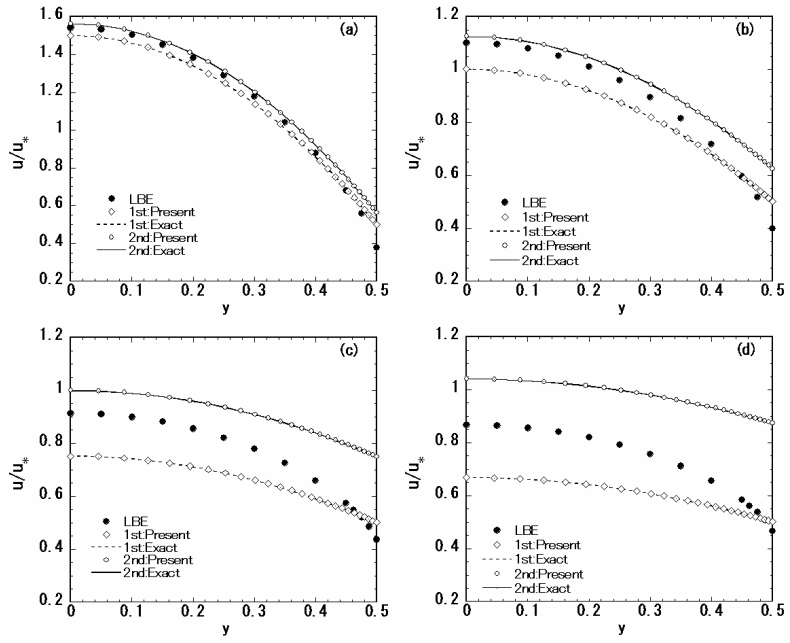

Fig. 2 Velocity profiles of the first and second-order slip boundaries. Present : Numerical solution, Exact : Eq. (13). (a) $k = 0.1$ (b) $k = 0.2$ (c) $k = 0.4$ (d) $k = 0.6$.

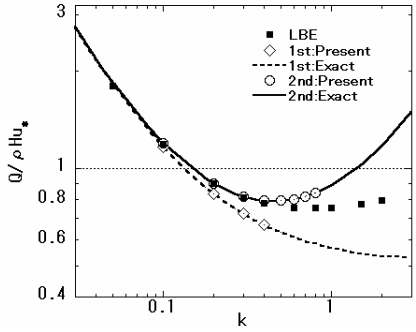

Fig. 3 Mass flow rate for the Poiseuille flow of the first and second-order boundary conditions. Present : Numerical solution, Exact : Eq. (14) with $\tilde{A}_2$, LBE : Ohwada *et al.*(1989) [21]

It has already been confirmed in Ref. 12 that the numerical solutions for the Maxwell's first-order slip condition $(A_1, A_2) = (1.0, 0.0)$ are in agreement with the LBE solution up to $k \cong 0.1$. In the present paper, numerical solutions by the present method for the pairs of the first-order $(A_1, A_2) = (1.11, 0.0)$ and second-order $(A_1, A_2) = (1.11, 0.61)$ slip velocity boundary conditions are compared again to the N-S exact solutions Eqs. (13) and (14) and Ohwada's LBE solutions.

Meanwhile, the contribution of the Knudsen layer to the mass flow rate Q_M has to be taken into consideration in second-order slip models, and the correct mean flow velocity has to be also modified as follows:

$$\langle u \rangle = \int_{-1/2}^{1/2} \left(u + \xi Kn^2 \frac{\partial^2 u}{\partial y^2} \right) dy = \int_{-1/2}^{1/2} u dy + \xi Kn^2 \left(\left. \frac{\partial u}{\partial y} \right|_{y=1/2} - \left. \frac{\partial u}{\partial y} \right|_{y=-1/2} \right), \tag{15}$$

where $\xi = 0.296$ for the HS model[24]. Hence, the exact mass flow rate Eq. (14) has to be also obtained by replacing A_2 with the effective coefficient $\tilde{A}_2 = A_2 - \xi (= 0.314)$. In obtaining the mass flow rate from the N-S numerical solutions, the trapezoidal rule and a second-order one-sided difference are used for the integral and the first-order spatial derivative on the walls at $y = \pm 0.5$ in the right-hand side of Eq. (15), respectively.

Figure 2 shows velocity profiles of the present method, the N-S exact solution Eq. (13)

for the first and second-order slip boundaries and the LBE. Numerical solutions by the present method are in very good agreement with Eq. (13) in any Knudsen numbers and the method can accurately give the "N-S" velocity solutions that are consistent with the slip boundary Eq. (6). It is found in Fig. 2 that the difference of solutions between the first-order and the second-order slip boundaries increases with increasing the Knudsen number owing to the second-order term in Eq. (6). However, the effectiveness of the second-order slip boundary condition can be found in all results of Fig. 2 as the discussion given by Hadjiconstantinou, who has suggested the effective thickness of Knudsen layer $\delta \cong 1.5\lambda$ [23]. For example, the thickness is estimated $\delta \cong 3/\sqrt{\pi}\, kH \cong 1.7kH$ in this problem. It can be seen in Fig. 2(a) and (b) that the second-order boundary is in better agreement with the LBE solution than the first-order boundary out of the Knudsen layer in $|y| \le \approx 0.3$ and $|y| \le \approx 0.15$ for $k = 0.1$ and $k = 0.2$, respectively; we can see second-order slip boundary conditions are effective to give true solutions out of the Knudsen layer as have been discussed in previous papers. However, the Knudsen layer covers a large part of the closed domain when k is larger than about 0.3, then, solutions by the N-S equation with the second-order slip boundary condition deviate from LBE solutions on the whole as shown in Fig. 2(c) and (d).

Figure 3 shows the comparison of numerical solutions of the flow rate for the first and second-order slip boundaries to Eq. (14). Note that the solution of the first-order boundary $(A_1, A_2)_1 = (1.11, 0.0)$ is almost identical with the first-order solution of the asymptotic theory for small Knudsen numbers $k << 1$ [15]. The LBE solutions in Ref. 21 are also displayed to be compared with the N-S solutions. Each numerical solution of the first and second-order slip boundary conditions is in good agreement with each exact N-S solution. In addition, it is confirmed that the solution of $(A_1, A_2) = (1.11, 0.61)$ agrees with the LBE up to $k \cong 0.3 (Kn \cong 0.4)$ as shown in Refs. 23 and 24. Cercignani has suggested the new effective coefficient $\widetilde{A}_2$ to make mass flow rate be consistent with the LBE solution; mass flow rate can be in good agreement with the LBE up to $Kn \cong 0.8$ [30]. However, it is not looked up in the present paper because this section is just devoted to validation of the present method for the N-S solution. Next, the present method is applied to two and three-dimensional cavity flows employing slip coefficients for the BGK model on the range of $Kn \le 0.1$.

3.2 Two-dimensional lid-driven cavity flow with slip velocity boundaries

Ghia *et al.* have given fundamental numerical solutions for a two-dimensional continuum cavity flow driven by the motion of a top wall using the incompressible N-S equations[31]; the solutions have been widely used to validate numerical schemes.

Naris and Valougeorgis have given the two-dimensional flow in the slip regime using the LBE[32], and Tang *et al.* have investigated them using the Lattice Boltzmann Method (LBM) for the discrete-velocity Boltzmann kinetic equation[33]. Mizzi *et al.* have obtained the solution of the Navier-Stokes-Fourier equations in conjunction with slip boundaries[34], and Darbandi *et al.* have done using a finite-volume-based finite-element method for the N-S equations[35]. One of the authors has also shown the two/three dimensional cavity flows in the slip regime $(Kn \le 0.1)$ using the Maxwell's first-order slip boundary condition $(A_1, A_2) = (1.0, 0.0)$. However, the flow of $Kn = 0.1$ was a little bit in disagreement with the result in Ref. 33. We revisit the flow with the second-order as well as the first-order boundaries.

The top wall speed u_W and the length (= the width) H of the cavity are taken as the reference speed U_0 and the reference length h_0, respectively. The top wall moves with a (nondimensional) constant speed $u_W = 1$ while the other three walls are stationary. The Reynolds number Re is fixed to 0.3 in this section, that is, Kn/Ma is also fixed by Eq. (3). Therefore, a mach number Ma also changes depending on a Knudsen number. For example, the real top wall speed for $Kn = 0.1$ is ten times higher than for $Kn = 0.01$ in the constant temperature T_0. However, the mach number is set to be very small as

$O(10^{-3})$ even in $Kn = 0.1$ so that the assumption of incompressible flows can be satisfied. The initial macroscopic velocity of the gas is $(u, v) = (0,0)$.

The number of grid points are $(N_x, N_y) = (50,50)$ and the computational regions are $(0 \le x, y \le 1.0)$. Both x and y spaces are divided into nonuniform sections with the minimum width $\Delta x_{\min} = \Delta y_{\min} = 6.175 \times 10^{-3}$ near the four walls and the maximum width $\Delta x_{\max} = \Delta y_{\max} = 4.568 \times 10^{-2}$ around the center of the cavity. These numerical conditions such as grid sizes are the same as what have been employed in the previous paper[12].

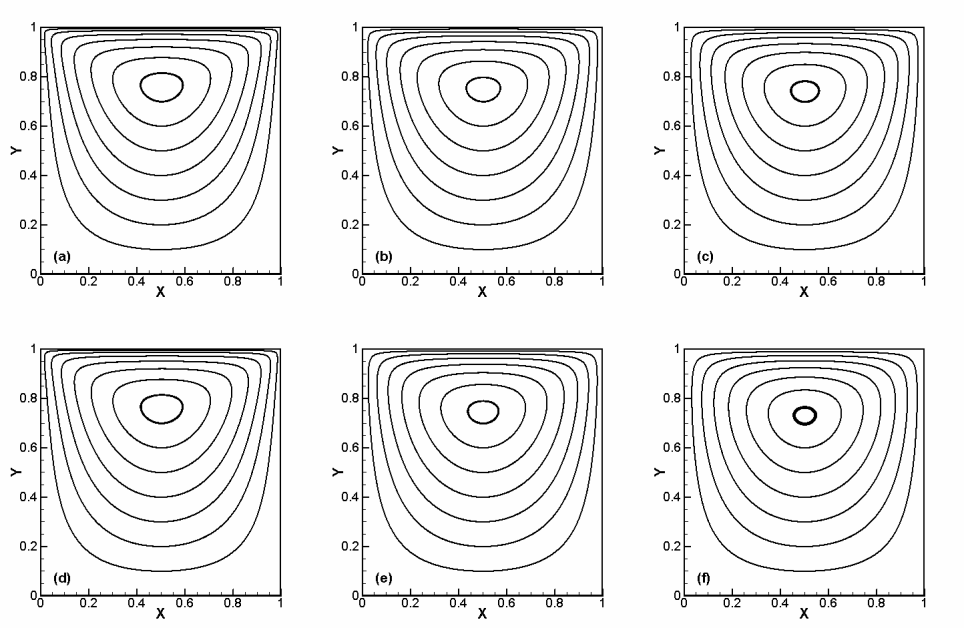

Fig. 4 Streamlines of the two-dimensional cavity flow in the slip regime. Top line (a)-(c) : $(A_1, A_2) = (1.0,0.0)$, Bottom line (d)-(f): $(A_1, A_2) = (1.1466,0.9756)$. (a)(d) $Kn = 0.01$, (b)(e) $Kn = 0.05$, (c)(f) $Kn = 0.1$.

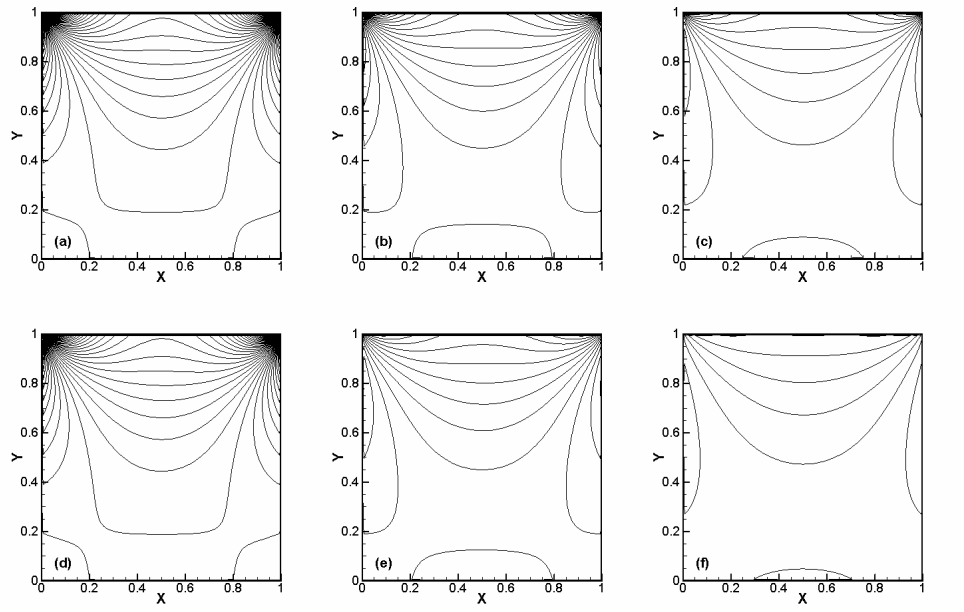

Fig. 5 Vorticity contours for both slip boundaries. Top line (a)-(c) : $(A_1, A_2) = (1.0,0.0)$, Bottom line (d)-(f) : $(A_1, A_2) = (1.1466,0.9756)$. (a)(d) $Kn = 0.01$, (b)(e) $Kn = 0.05$,(c)(f) $Kn = 0.1$ .The contour lines go from -32 to 10, 60 contours.

Coefficients $(A_1, A_2) = (1.1466,0.9756)$ are employed for the BGK model[20,34,35] to be

compared with the ones for the Maxwell's first order boundary $(A_1, A_2) = (1.0, 0.0)$[12] and Ref. 33. The coefficient $\alpha = \pi/4$ is used for the Reynolds number in Eq. (3).

Figures 4 and 5 display the comparison of the streamlines and the vorticity component q_z at steady states for $Kn = 0.01, 0.05$ and 0.1. The top and bottom lines of Figs. 4 and 5(a)-(c) and (d)-(e) are the solutions for the first and second-order boundary conditions, respectively. The streamlines are symmetry about $x = 0.5$ because of the low Reynolds number. Kawaguchi has shown solutions of vorticities and streamlines for continuum flows at low Reynolds numbers[36], and the present solutions are also similar to the solutions.

Although the first-order boundary hardly differs from the second-order one in $Kn = 0.01$, differences appear in $Kn = 0.1$. For example, the streamlines of the second-order boundary become rounder around the top corners and the vortex center, and vorticity becomes weaken more than of the first-order owing to the effect of slip velocity on the flow. Such slip effects can be also recognized in Fig. 6, which shows the velocity profiles passing through the geometric center of the cavity. Numerical solutions of nonslip boundary and Ref. 33 are also depicted as references. The reference data is directly extracted from the figures in Ref. 33 with our careful checks.

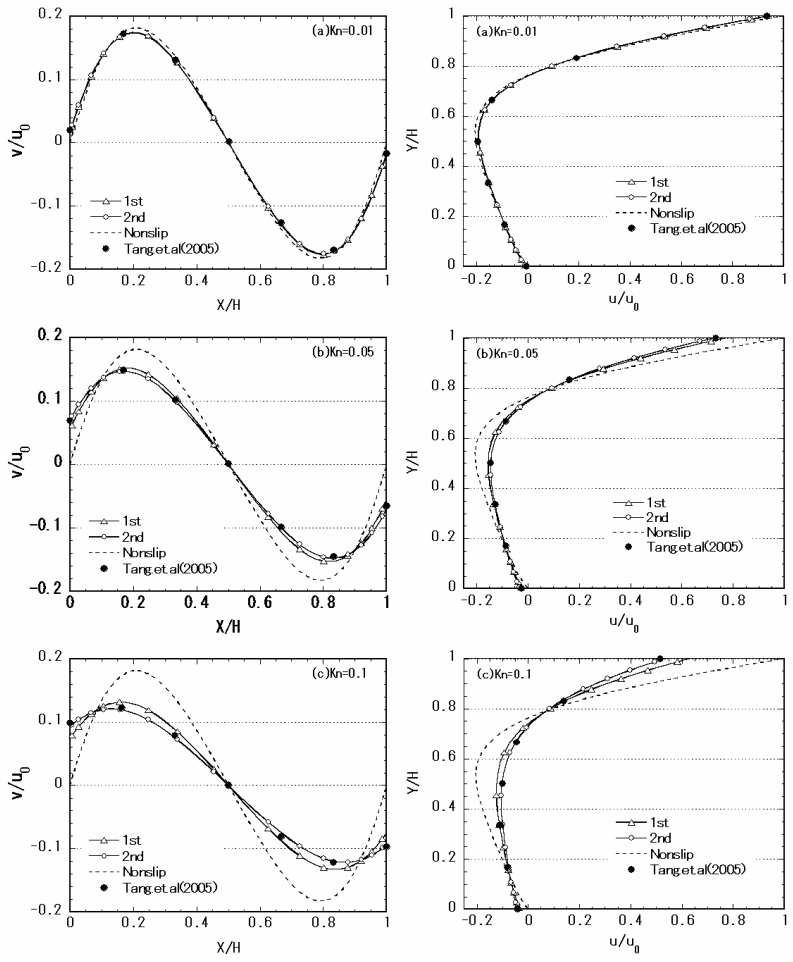

Fig. 6 Velocity profiles for various Knudsen numbers compared with Tang(2005)[33]. Left column: velocity v at $y = 0.5$, Right column: velocity u at $x = 0.5$.

The profiles in x and y-directions of both slip boundaries are almost the same as those of the nonslip flow in $Kn = 0.01$. On the contrary, while the first slip velocity deviates a little bit from Ref. 33, the whole profiles for the second-order slip boundary become in good agreement even in $Kn = 0.1$.

While a cavity flow is converged to a steady state in a low Reynolds number, tangential

gradients of velocity exist on all walls and the cavity has four corners unlike the Poiseuille flow. However, it is found that the general form of second-order boundary in the N-S equations is effective to a flow even in such a closed area on the adequate range of the Knudsen number as the previous section.

We have also tested the cubic-interpolation using four points instead of Eq. (7), for example, the condition of $u_{i,3}$ is added to Eqs. (8)-(10). However, no difference between Eq. (7) and the interpolation could be found in all results of Figs. 4 to 6. It goes to show that a coefficient of the third-order term in the interpolation is almost zero. The property is considered to be appropriate in general because boundary layer (not Knudsen layer) in N-S solution part u_{NS} is thick such as laminar flows in finite Knudsen numbers and small Mach numbers, that is, small Reynolds numbers, and slip effect most likely suppresses steep variation of tangential velocity profile near a wall in u_{NS} as shown in Figs. 2 and 6.

3.3 Three-dimensional lid-driven cavity flow with slip velocity boundaries

The last application is the three-dimensional lid-driven cavity flow. A lot of calculations for three-dimensional incompressible continuum flows in a cubic-cavity such as Ref. 37 have been examined, and Tang *et al.* have studied three-dimensional flows in a microduct using the Lattice Boltzmann model well lately[38]. However, there have been still few reports of three-dimensional slip flows. One of the authors has calculated the three-dimensional cavity flow using the Maxwell's first-order slip boundary. The present chapter compares both the first and second-order slip boundary conditions based on the BGK model as the previous section, and discusses differences of slip effects by end walls on whole flow fields between in two and three-dimensions.

The top wall speed u_W and the length (=the width and the depth) H of the cubic cavity are taken again as the reference speed U_0 and the reference length h_0, respectively. The computational regions of the cubic cavity are $(0 \le x, y, z \le 1.0)$ and the number of grid points are $(N_x, N_y, N_z) = (50,50,50)$. The same way to locate grid points as the two-dimensional case is employed; all three directions are divided into nonuniform sections with the minimum width $\Delta x_{\min} = \Delta y_{\min} = \Delta z_{\min} = 6.175 \times 10^{-3}$ near the six walls and the maximum width $\Delta x_{\max} = \Delta y_{\max} = \Delta z_{\max} = 4.568 \times 10^{-2}$ around the center of the cubic cavity. The top wall at $z = 1$ moves in x-direction with a constant speed $u_W = 1$, and the other five walls are stationary. The Reynolds number Re is fixed to 0.3 again, and each mach number Ma for each Knudsen number Kn is also the same as that in the two-dimensional cavity flow. Slip coefficients $(A_1, A_2) = (1.0,0.0)$ and $(A_1, A_2) = (1.1466,0.9756)$ are taken for the first and second-order slip boundary conditions, respectively.

Figure 7(a)-(d) shows streamlines, in which five and three cross sections are depicted from $y = 0$ to $y = 1$ at steady states for the second-order slip $(A_1, A_2) = (1.1466,0.9756)$ and nonslip flows, respectively. The streamlines are also shown on two end walls $y = 0$ and $y = 1$ for the slip flows. All streamlines are symmetric about the plane $x = 0.5$ as two-dimensions. While the difference between Figs. 7(a) and 7(b) can be hardly seen inside the cavity as a result of the small slip effects on the flow of $Kn = 0.01$, streamlines on all cross sections become round with increasing the Knudsen number in Fig. 7(c) and (d) as discussed in the two-dimensional cases.

Figure 8(a)-(f) shows the comparison of vertical velocity component to the bottom wall (w) at the plane of symmetry $y = 0.5$ to the component in two-dimensions (v) for the nonslip and $Kn = 0.1$ for the first and second-order boundaries. Although differences of physical quantities such as streamlines have been discussed between the first and second-order boundaries in the two-dimensions, differences can be hardly found between two-dimensions and the plane of symmetry in three-dimensions for both slip boundaries even in rather large $Kn = 0.1$. The results have indicated that, even if end walls also exist in slip flows, the velocity profile at the mid-plane are hardly changed like Stokes flows in low Reynolds numbers; the discussion of $Re = 100,400$ and 0.02 for continuum flows with

the nonslip boundary have been given in Ref. 39.

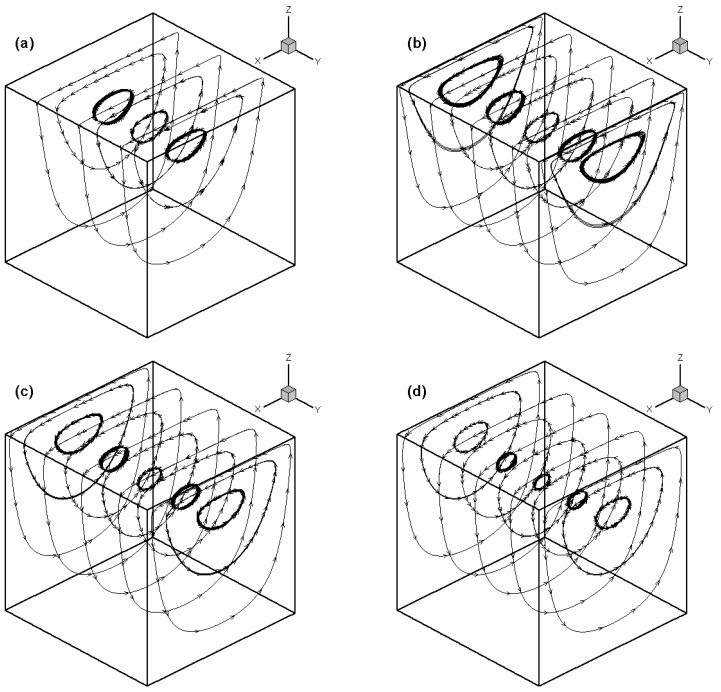

Fig. 7 Streamlines for the second-order slip and nonslip boundary conditions. (a) Nonslip (b) $Kn = 0.01$ (c) $Kn = 0.05$ (d) $Kn = 0.1$.

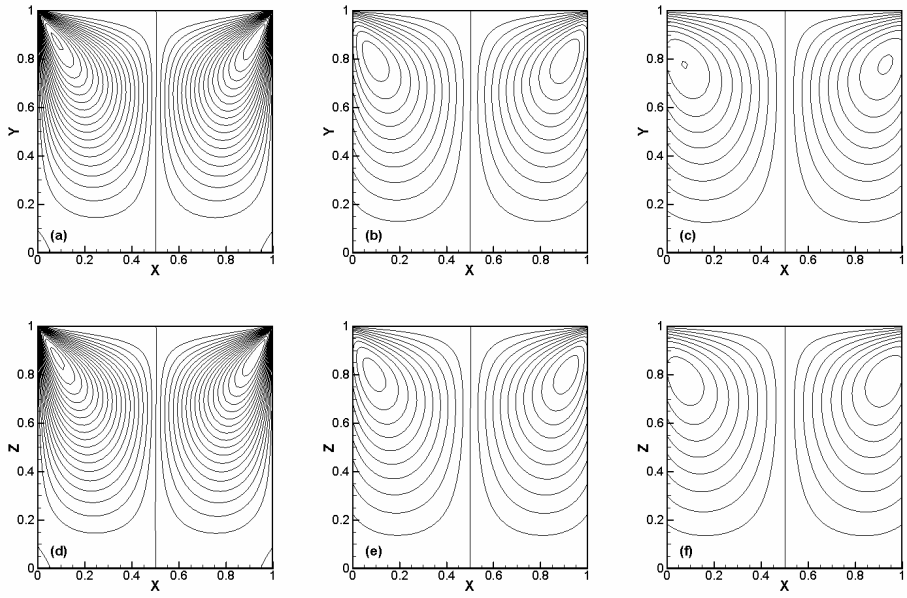

Fig. 8 Vertical velocity component to the bottom wall for 2-D (Top line) and the plane of symmetry in 3-D (Bottom line). (a)(d) Nonslip, (b)(e) $Kn = 0.1$ for $(A_1, A_2) = (1.0, 0.0)$, (c)(f) $Kn = 0.1$ for $(A_1, A_2) = (1.1466, 0.9756)$. The contour lines go from -0.38 to 0.38, 39 contours.

However, slip effects on walls can be clearly seen in Figs. 9 and 10 (a)-(d) which show contour slices of x and z-components of velocity (u, w) at $y = 0.0, 0.5$ and 1.0, respectively. The maximum value of y-component (v) is over one order of magnitude lower than the other two components. The contours on the end plates $y = 0$ and $y = 1$ become clear with increasing the Knudsen number while there are no or only a few contour lines in nonslip or the small Knudsen number flows. In particular, the contours on the end

plates become similar to the one on the plane of symmetry for $Kn = 0.1$ because of the large slip effect on the walls. The effect can be also compared in Fig. 11(a) and (b) which depict the profiles of velocity u at the center of xy-plane $(x = y = 0.5)$ and xz-plane $(x = z = 0.5)$, respectively in the second-order boundary of (A_1, A_2); the line $x = z = 0.5$ is below the center of the primary vortex. Figure 4 can be also referred by the following discussion.

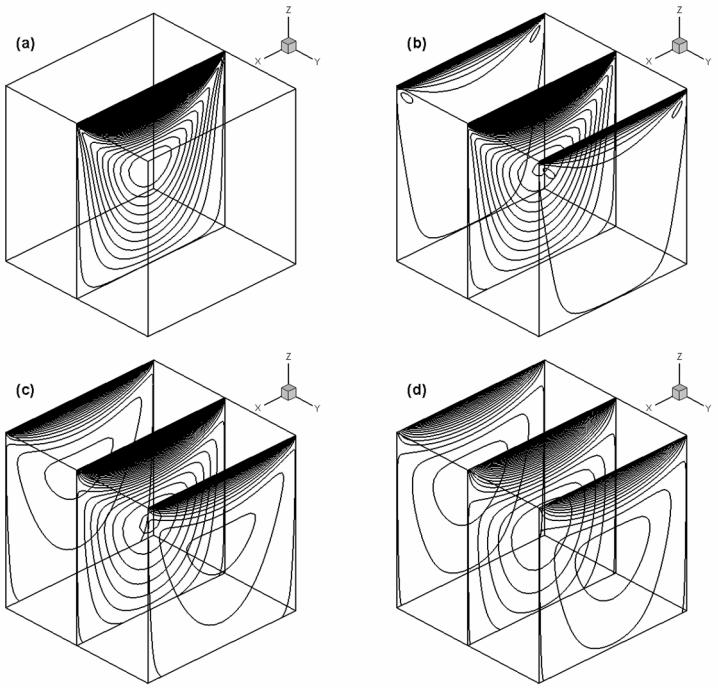

Fig. 9 Contour slices of x-component of velocity (u) for the second-order slip and nonslip boundary conditions. (a) Nonslip, (b) $Kn = 0.01$, (c) $Kn = 0.05$, (d) $Kn = 0.1$. The contour lines go from -0.2 to 1.0, 60 contour lines.

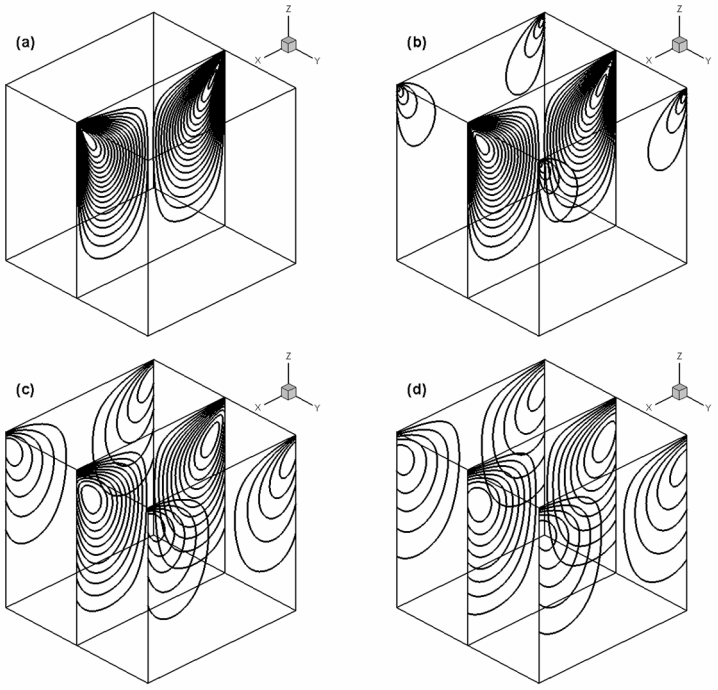

Fig. 10 Contour slices of z-component of velocity (w) for the second-order slip and nonslip boundary conditions. (a) Nonslip, (b) $Kn = 0.01$, (c) $Kn = 0.05$, (d) $Kn = 0.1$. The contour lines go from -0.38 to 0.38, 39 contour lines.

The three-dimensional results in Fig. 11(a) are compared with the two-dimensional ones. It can be found in Fig. 11(a) that the profiles of three-dimensions at the plane of symmetry $y = 0.5$ is almost the same as those of two-dimensions in $Kn = 0.05$ and $Kn = 0.1$ as mentioned in Fig. 8, though small difference can be seen at $z \cong 0.5$ in $Kn = 0.01$ which rather corresponds to a continuum flow. In addition, while each profile in Fig. 11(b) is symmetry about $y = 0.5$, the flow speed around $y = 0.5$ becomes low but the one on both walls $y = 0$ and $y = 1$ becomes high owing to the slip as the Knudsen number increases. Thus, the large slip effect on end walls makes the velocity profile gradually approach flat. Figure 11(b) has indicated that the slip effect caused by the walls spreads in the cavity, then, the flow gradually becomes two-dimensional on the whole as Figs. 9, 10 and 11(a) with increasing the Knudsen number.

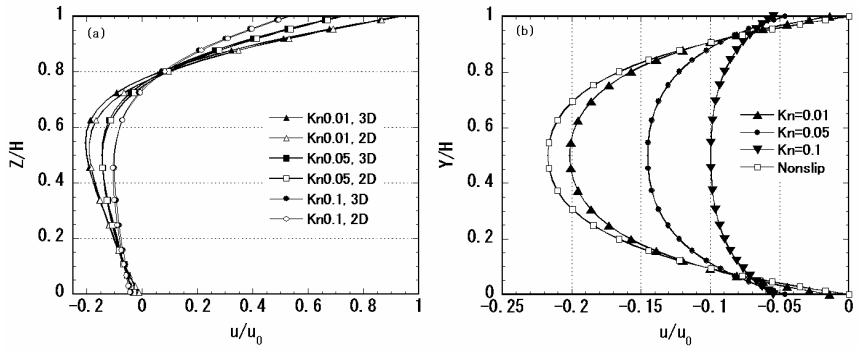

Fig. 11 Velocity profiles of u by the second-order boundary condition for various Knudsen numbers. (a) $x = y = 0.5$ (b) $x = z = 0.5$.

4. Concluding remarks

We have presented a numerical scheme using the CIP method for slip flows solved with the incompressible Navier-Stokes equations in conjunction with a general form of slip boundaries. The approach can be applied to the HS and BGK models by changing slip coefficients (A_1, A_2) as well as the definitions of viscosity or the Reynolds number. Numerical experiments have indicated that the present method for both first and second-order boundary conditions can give reasonable numerical solutions on the range of Knudsen numbers $Kn \le O(10^{-1})$. While the tangential velocity on the wall is determined by only two grid points above the wall, the whole profile can be obtained without any discrepancy. Differences of velocity slip effects by first and second-order slip boundaries appear in not only the Poiseuille flow in an open area but also the lid-driven cavity flow in a closed area. In particular, in three-dimensional cavity flows, end walls with large slip effects make flow structure changed like two-dimensions in the large Knudsen number.

Though the approximation Eq. (7) is not on the basis of physics, not less than a quadratic polynomial of coordinate n is needed to represent a non-zero second-order derivative in Eq. (6); a linear interpolation can deal with only a first-order slip boundary. For example, Eq. (7) is proved to be valid in the plane Poiseulle flow; Eq. (7) can give its exact solution in the N-S equations. On the contrary, higher-order interpolations than Eq. (7) might be also needed in general, such as a cubic interpolation used well for laminar boundary layer on a simple plane. However, we have found Eq. (7) is sufficient while higher-order interpolation functions can be formally made using more than three grid points. Velocity of the N-S part u_{NS} of a slip flow varies smoothly compared to a continuum flow in laminar boundary layer as shown in the present paper. Hence, higher-order terms are much smaller than the second-order term because coefficients of higher-order terms are not very large as discussed in Section 3.2, and Eq. (7) is applied in a short range of coordinate $n << 1$ when fine mesh is set near a wall; the range is much

smaller than the reference length. Therefore, even if the third-order term such as $A_3 Kn^3 \left(\partial^3 u/\partial n^3\right)_{\mathbf{x}=\mathbf{x}_W}$ could be added to Eq. (6), the term would be also negligible in slip regime $Kn \approx O\left(10^{-1}\right)$ because the third-order derivative becomes small on a wall; higher-order terms than the second-order term are clearly negligible in very small Knudsen numbers.

When thickness of the Knudsen layer increases, not only the quadratic as Eq. (7) but also higher-order interpolation functions are still insufficient to determine the true velocity profile in the layer as mentioned in Section 3.2. Lockerby *et al.* have discussed wall functions to approximate the flow profile of the Knudsen layer part u_{Kn} [25]; it makes true velocity profiles u_{true} largely deviated from u_{NS} with increasing the Knudsen number. Such approach is similar to what is used in turbulent boundary-layer modeling, and the approach can be probably one of solutions to be included in slip boundary conditions.

The present scheme also warrants extensions to the other type of slip boundaries, general surface geometries with curvature κ, and moving bodies for wide applications to microdevices such as micro pumps[40]. While the CIP method can be applied to curvilinear coordinates[41], tangential shear stress for arbitrary body shapes has to be exactly included in slip boundaries. However, the present formulation for the slip boundary can be applied to the cylindrical and spherical coordinates because the tangential shear stress can be exactly expressed. The extension to curved surfaces and three-dimensional practical applications will be reported as our next future works.

Acknowledgment

We would like to thank to Professor Hiroshi Maekawa of the University of Electro-Communications for his support.

References

(1) Bird, G. A., *Physics of Fluids*, Vol.6(1963), pp.1518-1519.
(2) Bird, G.A., *Molecular Gas Dynamics and the Direct Simulation of Gas Flows*. Oxford Science, Oxford(1994).
(3) Sone, Y., Tanaka, S., and Ohwada, T., *European Journal of Mechanics, B/Fluids*,Vol.9 (1990), pp.273-288.
(4) Ohwada, T., *Physics of Fluids A*, Vol.5 (1998), pp.217-234.
(5) Bhatnagar, P. L., Gross, E. P, and Krook, M., *Physical Review*, Vol.94(1954), pp.511-525.
(6) Karniadakis, G., Beskok, A., and Aluru, N., *Microflows and nanoflows,* Springer(2005)
(7) Gad-el-Hak, M., *ASME Journal of Fluids Engineering,* Vol.121 (1999), pp.5-33.
(8) Struchtrup, H., *Macroscopic transport equations for rarefied gas flows,* Springer(2005).
(9) Maxwell, J. C., *Philosophical Transactions of the Royal Society of London,* Vol.170 (1879), pp.231-256.
(10) Yabe, T., and Aoki, T., *Computer Physics Communications,* Vol.66 (1991), pp.219-232.
(11) Yabe, T., Xiao, F., and Utsumi, T., *Journal of Computational Physics,* Vol.169(2001), pp.556-593.
(12) Ogata, Y., and T, Kawaguchi., *Journal of Fluid Science and Technology,* Vol.6(2011), pp.215-229.
(13) Shen, C., *Rarefied gas dynamics, fundamentals, simulations and micro Flows*, Springer, (2005).
(14) Sone, Y., *Kinetic Theory and Fluid Dynamics*. Birkhäuser(2002).
(15) Sone, Y., *Molecular gas dynamics, Theory, Techniques, and Applications*. Birkhäuser, (2007).
(16) Yabe, T., and Wang, P.Y., *Journal of the Physical Society of Japan,* Vol.60(1991), pp.2105-2108.

(17) Xiao, F., Yabe, T., Nizam, G., and Ito, T., *Computer Physics Communications,* Vol.94 (1996), pp.103-118.
(18) Takewaki, H., and Yabe, T., *Journal of Computational Physics,* Vol.70(1987), pp.355-372.
(19) Yabe, T., Ogata, Y., and Takizawa, K., *International Conference on Computational Fluid Dynamics(ICCFD)4, Ghent, Belgium*(2006), pp.29-43.
(20) Cercignani, C., *Institute of Engineering Research Report AS-6419*(1964), *Univ. of California.*
(21) Ohwada, T., Sone, Y., and Aoki, K., *Physics of Fluids A,* Vol.1(1989), pp.2042-2049.
(22) Hsia, Y.-T., and Domoto, G. A., *ASME Journal of Lubrication Technology,* Vol.105(1983), pp.120-130.
(23) Hadjiconstantinou,N.,G., *Microscale Thermophysical Engineering,* Vol.9(2005), pp.137-153.
(24) Hadjiconstantinou, N, G., *Physics of Fluids,* Vol.15(2003), pp.2352-2354.
(25) Lockerby, D. A., Reese, J. M., and Gallis, M. A., AIAA *Journal,* Vol.43(2005), pp.1391-1393.
(26) Sone, Y., *Rarefied Gas Dynamics,* Academic Press, New York, Vol.1(1969), pp.243-253.
(27) Sone, Y., *Rarefied Gas Dynamics,* Editrice Tecnico Scientifica, Pisa, Vol.2(1971), pp.737-749.
(28) Weng H.C., and Chen C-K., *Phys.Fluid,* Vol.20(2008), pp.106101-1-9.
(29) Aoki, K., Takata, S., and Aikawa, H., *Physics of Fluids,* Vol.13 (2001), pp.2645-2661.
(30) Cercignani, C., and Lorenzani, S., *Physics of Fluids,*Vol. 22 (2010), pp.062004-1-8.
(31) Ghia, U., Ghia, K. N., and Shin, C. T., *Journal of Computational Physics,* Vol.48(1982), pp.387-411.
(32) Naris, S. and Valougeorgis, D., *Physics of Fluids,* Vol.17(2005), pp.097106-1-12.
(33) Tang, G. H., Tao, W. Q., and He, Y. L., *Physics of Fluids,* Vol.17(2005), pp.058101-1-4.
(34) Mizzi, S., Emerson, D. R., Stefanov, S. K., Barber, R. W., and Reese, J. M., *Journal of Computational and Theoretical Nanoscience,*Vol. 4(2007), pp.817-822.
(35) Darbandi, M., Daghighi, Y., Vakilipour, S., and Schneider, G. E., *48th AIAA Aerospace Sciences Meeting and Exhibit, Reno, Nevada*(2008), pp.1-13.
(36) Kawaguchi, M., *Journal of the Physical Society of Japan,* Vol.16(1961), pp.2307-2315.
(37) Jiang, B-N., Lin, T. L., and Povinelli, L. A., *Computer Methods in Applied Mechanics and Engineering,* Vol.114(1994), pp.213-231.
(38) Tang, G. H., Tao, W. Q., and He, Y. L., *Journal of Applied Physics,* Vol.97(2005), pp.104918-1-8.
(39) Takami, H. and Kuwahara, K., *Journal of the Physical Society of Japan,* Vol.37(1974), pp.1695-1698.
(40) Lockerby, D. A., Reese, J. M., Emerson D. R., and Barber, R. W., *Physical Review E,* Vol.70(2004), pp.017303-1-4.
(41) Wang, P.Y, Yabe, T., and Aoki, T., *Journal of the Physical Society of Japan,* Vol.62(1993), pp.1865-1871.